Data from thermal testing of the Open Source Cryostage

Buch, Johannes Lørup; Ramløv, Hans

Published in:
Data in Brief

DOI:
10.1016/j.dib.2016.06.056

Publication date:
2016

Document Version
Publisher's PDF, also known as Version of record

Citation for published version (APA):
Buch, J. L., & Ramløv, H. (2016). Data from thermal testing of the Open Source Cryostage. *Data in Brief*, *8*, 885-890. https://doi.org/10.1016/j.dib.2016.06.056

Cryobiology 72 (2016) 251–257

Contents lists available at ScienceDirect

Cryobiology

journal homepage: www.elsevier.com/locate/ycryo

An open source cryostage and software analysis method for detection of antifreeze activity

J.L. Buch [a, *], H. Ramløv [b]

[a] Department of Biology, University of Southern Denmark, Campusvej 55, 5230 Odense M, Denmark
[b] Department of Science and Environment, Roskilde University, Universitetsvej 1, 4000 Roskilde, Denmark

ARTICLE INFO

Article history:
Received 3 December 2015
Received in revised form
26 March 2016
Accepted 28 March 2016
Available online 31 March 2016

Keywords:
Antifreeze protein
Recrystallisation
Cryostage
Microscopy
Detection

ABSTRACT

The aim of this study is to provide the reader with a simple setup that can detect antifreeze proteins (AFP) by inhibition of ice recrystallisation in very small sample sizes. This includes an open source cryostage, a method for preparing and loading samples as well as a software analysis method. The entire setup was tested using hyperactive AFP from the cerambycid beetle, *Rhagium mordax*. Samples containing AFP were compared to buffer samples, and the results are visualised as crystal radius evolution over time and in absolute change over 30 min. Statistical analysis showed that samples containing AFP could reliably be told apart from controls after only two minutes of recrystallisation. The goal of providing a fast, cheap and easy method for detecting antifreeze proteins in solution was met, and further development of the system can be followed at https://github.com/pechano/cryostage.

1. Introduction

Organisms vary in their response to cold and freezing conditions. Some are tolerant to internal freezing, while others must avoid it to survive. Insects have a variety of behavioural responses to initially avoid the cold [24,20], but evolution has in many cases favoured the adaptation of a physiological cold response [28,19]. Plants indigenous to the temperate regions of the world often experience freezing conditions for extended periods of time, but their inability to move leaves them few options for freeze avoidance through behaviour [7,26]. For many organisms, freeze tolerance is therefore an important survival strategy. Freeze tolerant organisms typically do not freeze completely at random. Rather, the freezing process is directed by biological ice nucleating agents [20,21,29,30], found in blood and tissue. For most freeze tolerant organisms, intracellular freezing is still unwanted and damaging [26], and thus extracellular ice nucleation prevents fatal damage. Freeze avoiders often employ a certain group of biological antifreeze agents called antifreeze proteins (AFP),[1] as well as low molecular weight colligative antifreeze compounds such as polyols [34], free amino acids [20] and inorganic salts [27].

Due to biological constraints, the colligative antifreeze response only has a functional range down to a maximum of −10 °C in most species. Further protection from freezing must be provided by AFP [27,32]. Tiny ice crystals that may otherwise inoculate the supercooled body fluid are effectively neutralised through a process known as adsorption inhibition [22]. The mode of action is believed to be a function of the Kelvin effect [16], which states that vapour pressure of a surface is correlated to it's curvature. See Eq. (1) below. As the particle radius r decreases, surface vapour pressure increases due to curvature. The effect of curvature on surface vapour pressure also relates to the ice nuclei that constantly form at random in an undercooled solution. If the radius, r, is below a certain value, phase equilibrium will shift towards the liquid and the nucleus dissolves. This effect is exploited by AFP on the surface of ice crystals.

$$ln\frac{p}{p_0} = \frac{2\gamma V_m}{rRT} \quad (1)$$

where.

p: vapour pressure of surface
p_0: vapour pressure of solution

* Corresponding author.
E-mail addresses: jloerup@gmail.com (J.L. Buch), hr@ruc.dk (H. Ramløv).

[1] As more intricate knowledge about the mechanism of these proteins have become available in recent years, they are often referred to as **I**ce **B**inding **P**roteins or **I**ce **S**tructuring **P**roteins.

http://dx.doi.org/10.1016/j.cryobiol.2016.03.010
0011-2240/

γ: surface tension
V_m: molar volume
r: crystal radius
T: system temperature in Kelvin
R: universal gas constant

AFP adsorb irreversibly onto the ice crystal surface and prevent ice from forming underneath it [16]. Between adsorbed AFP, the ice crystal will continue to grow as a convex bulge with the minimum radius r. A denser population of adsorbed AFP will lead to lower r, which increases the vapour pressure of the convex surfaces between adsorbed AFP (Eq. (1)). This shifts the interfacial phase equillibrium towards the liquid state, effectively preventing further ice crystal growth at a given temperature. If the temperature is lowered further, the equillibrium shifts towards the crystal phase, slowly expanding the crystal with decreasing temperature. At a certain temperature, the effect breaks down and an explosive crystal growth is observed [25]. In the metastable system consisting of liquid water and tiny ice crystals, the temperature difference between the equillibrium melting point T_m and the non-equillibrium freezing point, where the antifreeze effect breaks down, is called thermal hysteresis, *TH*.

In freeze avoiding organisms, the primary function of AFP is allowing body fluids, despite the presence of tiny ice crystals, to become supercooled through thermal hysteresis. AFPs are often found in freeze tolerant organisms as well [21]. This may seem paradoxical, but is often attributed to their secondary function, which is inhibition of recrystallisation, *RI*. As an aqueous solution freezes, it often happens from several nucleation points, especially if the rate of cooling is high. A slow freezing may result in fewer nucleation points, or even just one single point of nucleation. This is typically seen in ice cubes or the surface of a frozen pond during a cold spell, both examples of finely structured ice crystals. If a large number of nucleation points initialise ice crystal growth, the final body of ice consists of a varied distribution of ice crystal orientations and sizes [14]. Variations in radius equals variation in surface vapour pressure. This leads to the phenomenon known as Ostwald ripening, which is the mechanism that drives recrystallisation of ice [3]. When water freezes, solutes are exclude from the growing crystal, leading to a sharp concentration gradient near the crystal surface. In a flash frozen sample with many tiny ice crystals, the macroscopic distribution of solutes is not significantly different from a liquid system. As time passes and Ostwald ripening is allowed to recrystallise the ice, larger and larger areas of the ice cross section will be either pure ice or pure brine, see Fig. 1. It is this clear separation between ice and its surroundings that is the basis for the detection method described in this paper. For the purpose of the method, bulk-ice and edge-ice, will henceforth refer to the large surface of the growing ice-crystal and the interfacial region in contact with water, respectively.

The recrystallisation process is believed to be a main cause of tissue damage in frozen organisms [11,5]. By inhibiting recrystallisation in frozen body fluids, AFP's can essentially extend the period of time before permanent damage occurs from freezing of tissue.

From an industrial point of view, recrystallisation has a significant impact on quality of frozen goods. Reducing the amount of recrystallisation that takes place in frozen storage of foodstuffs could therefore be of interest. Zang et al. [33] showed that addition of carrot AFP to frozen dough significantly improved frozen shelf life. The unfulfilled potential of AFP as a food additive is largely due to production issues, and as such, a new approach is perhaps in order. Naturally occurring AFPs from fish, and especially insects, have high antifreeze activity ratings in terms of thermal hysteresis. Several patents exist on both fish and insect AFP because of this. Plant antifreezes are different in the way that most do not provide a noticeable thermal hysteresis, but a rather efficient recrystallisation inhibition [8,9,17]. A potential source for future applications could be naturally occurring plant AFP.

Since the discovery of antifreeze proteins and the first quantification of their effects, thermal hysteresis has been used as an endpoint measurement for detection and activity. Thermal hysteresis activity, THA, shows a correlation to AFP concentration. There is no general formula to describe the concentration/effect relationship of all AFP's, but a functional calculation can be established on a case-to-case basis [16].

The inhibition of recrystallisation requires AFP concentrations orders of magnitude lower than detectable THA. So as a detection endpoint, IRI seems superior to THA. The effect is, however, somewhat binary over a large span of concentrations. Either there is complete IRI or there is none. This proves a challenge in terms of quantifying the effect, especially when compared to inorganic recrystallisation inhibitors, which provide a scalable inhibition over a large span of concentrations [18]. Screening for thermal hysteresis requires a time consuming and expensive setup that often includes a nanoliter osmometer. Screening for recrystallisation inhibition is different due to the nature of the mechanism. One only needs to observe ice crystals at a constant temperature for a limited amount of time to identify the presence of recrystallisation inhibition proteins.

In the past, IRI has been observed and quantified by microscopy [12,14,21]. Small samples of solution possibly containing AFP have been flash frozen and evaluated over time, by hand. There have been several method developments that automate some of the steps involved in detecting antifreeze activity, and reduce the amount of experimental sample needed. This paper seeks to combine the two ideals in order to provide the reader with a simple, low-cost setup for performing the experiments needed to

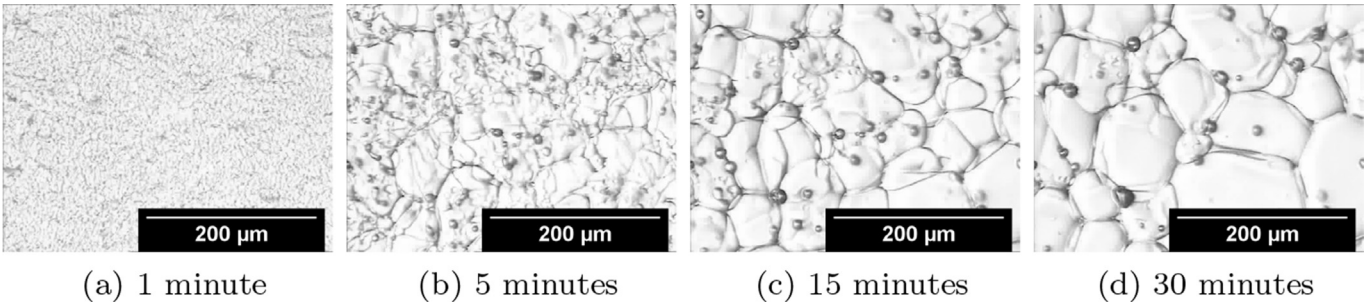

Fig. 1. Ostwald ripening or ice recrystallisation. All images are the same FOV at different points in time. The amount of edge-ice decreases with time, while the amount of bulk-ice increases. This mechanism is exploited as a detection method.

detect AFP and an automated data analysis workflow, using free software.

A study by Jackman et al. [13] showed that it was possible to use semi-automated software recognition of growing crystals in a microscope sample. By defining crystal boundaries in the software, crystal growth, or lack thereof, could be recognised by a computer programme. The algorithm was based around domain recognition, which determines the sizes of the largest ten crystals in a field of view, FOV. Budke et al. [3,4], showed that software recognition of crystals was indeed a viable approach, and that quantification of recrystallisation should be done using methods similar to theirs. A recent study by Hagiwara & Aumatsu, (2015) [10], likewise showed that it is possible to construct a low-cost cryostage, fitting for recrystallisation experiments. Braslavsky et al. [1] showed a LabVIEW controlled cryostage, capable of measuring TH, using a commercial temperature controller.

This paper presents an open source software analysis method and open source cryostage (OSC) design, that work in combination to allow detection of antifreeze proteins through recrystallisation inhibition.

2. Materials and methods

2.1. Microscope setup

Recrystallisation assays were performed using the OSC of our own design. A Clifton nanolitre osmometer (Clifton Technical Physics, Hartford, NY USA) was also used as a cryostage for comparison of results. The osmometer and OSC were placed under a Zeiss STEMI SV11 APO microscope with a Sony SVT-S 3050 P S-VHS camera connected to the light path. The camera feed was captured over S-VHS using a Pinnacle DC10plus, Motion-JPEG VideoIO Board. The S-VHS signal was routed via a small monitor for observing recrystallisation in real time. Illumination for the Clifton experiments was provided by a Schott KL1500 LCD, position 4B. The OSC was outfitted with a bright 20 mW LED beneath the sample holder.

2.2. Open source cryostage

A 60W Peltier (THR-DS-SH14,125,06,L1,W4.5-0509) unit was mounted on an aluminium heatsink, hot side down. The heatsink had internal channels that allowed cooled liquid to flow though, essentially keeping it at a constant set temperature of maximum 5 °C. At the center of the heatsink, a small hole (Ø = 5 mm) was drilled to allow for insertion of a bright LED to work as a light source for brightfield microscopy. The heatsink and Peltier unit were sealed inside an aluminium chassis. To allow sample loading, a small rectangular hole was milled right above the center of the Peltier unit. This hole was covered by a coverslip during experimentation to prevent condensation on the sample. A small rubber tube connected to a dry air pump was also introduced to the sample chamber during experiments, again to reduce condensation. See figure Fig. 2. The Peltier unit was connected to a 12 V 5 A power supply and power was modulated using 8-bit PWM through an IRL540N N-channel MOSFET, see Fig. 3 in Ref. [2].

Using Brett Beauregard's PID algorithm,[2] the Arduino was programmed for three different setpoint temperatures. Load (PWM = 0), Deep freeze (PWM = 255) and 90% ice, which depends on the sample osmolality. See 8.4 for details. A 100k NTC thermistor was used as input for the PID algorithm. The thermistor was placed between the Peltier unit and the first layer of insulation, close to the sample holder. The position corresponds to "J" in Fig. 2.

[2] https://github.com/br3ttb/Arduino-PID-Library.

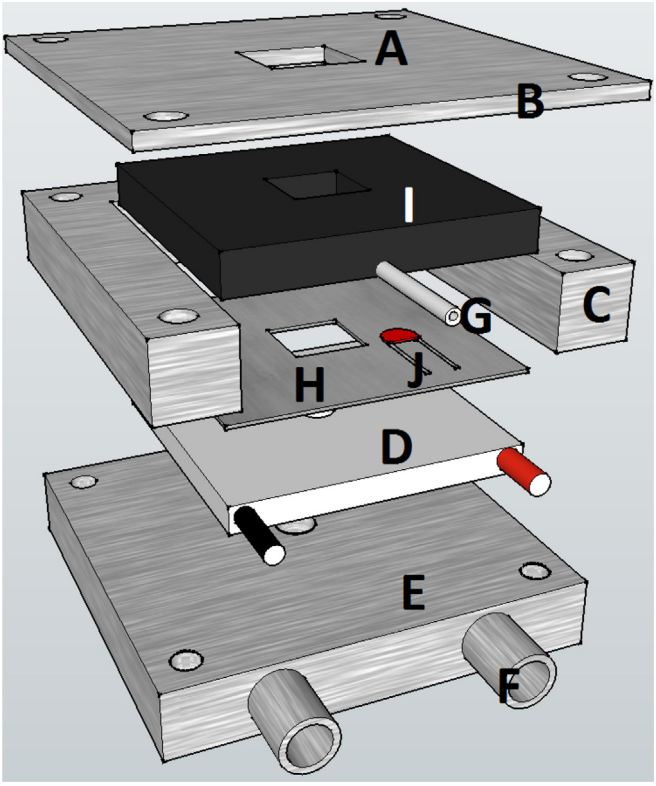

Fig. 2. Schematic drawing of the cryostage. A: Opening for loading and viewing sample. Covered by coverslip during experiments, B: Top aluminium plate that covers the Peltier unit, C: Middle chassis that functions as a thermal mass, D: Peltier unit, E: Heatsink, covered with thermal paste under the Peltier unit, F: Cold water intake for heatsink, G: Dry air intake, H: Aluminium heat spreader sheet, I: Foam insulation, J: 100K NTC thermistor.

2.3. Samples used

Three sample types were tested on the setup. 1: Recombinant RmAFP1 solution diluted with control PBS to 4 μg/ml (henceforth rmAFP256) and; 2: 0.5 μg/ml (henceforth rmAFP2048). 3: PBS Control solution with no antifreeze activity. AFP was prepared according to [15]. The specific AFP concentration of rmAFP256 was chosen because initial experiments showed that it was practically impossible to quantify thermal hysteresis, but that AFPs were clearly still present. The recombinant rmAFP used in this study was prepared following the method presented in Refs. [6,15].

Control samples containing no recrystallisation inhibiting agent were made from standard laboratory PBS containing no potassium. Osmolality was 311 mOsm/kg. All samples were done in at least duplicates and the results are represented as mean ± SD. All experiments were performed at 90% ice according to Eq. (2) [31].

$$F_i = 1 - \frac{T_0 - T_m}{T_0 - T_i} \tag{2}$$

where.

F_i: ice fraction
T_m: equilibrium melting point of solution
T_i: temperature of partially-frozen solution
T_0: equilibrium melting point of pure water, 273.15 K

For the control solution with an osmolality of 311 mOsm/kg, the desired F_i is reached at −5.78 °C. The freezing point depression was

first calculated using Eq. (3)

$$\Delta T_f = K_f * m \quad (3)$$

where.

ΔT_f: freezing point depression in Kelvin
K_f: cryoscopic constant of water
m: osmolality of solution

The depression is then used to calculate the new melting point, $T_m(T_0 - \Delta T_f)$.

$$\Delta T_f = 0.311 * 1.86 = 0.578K$$

$$T_m = T_0 - \Delta T_f$$

$$T_m = -0.578^{\circ}C$$

Which is inserted into Eq. (2) with a desired F_i of 90%. In Celsius:

$$0.9 = 1 - \frac{0.578}{-T_i}$$

$$0.9 - 1 = -\frac{0.578}{-T_i}$$

$$T_i = -\frac{0.578}{0.1}$$

$$T_i = -5.78^{\circ}C$$

This calculation was done for every sample to ensure homogeneity of F_i throughout the study. 90% was chosen because it ensures a moderate water flux near the ice crystals while still being within the operational parameters of the cooling device.

2.4. Data capture and processing

Briefly, all data points were captured as video and analysed as individual frames. Each frame was analysed for cross sectional area of "bulk" and "edge" and changes in these over time. The final result after processing is the evolution of the largest ice crystal radius within the FOV during the experiment.

2.4.1. Capture and compression with FFMPEG

Data was captured as a raw MPEG through the capture card and encoded to MPEG4 using the h264 video codec, see 8.1 for details. All capture was done through the free software package, FFMPEG.[3] On the basis of initial testing, an experimental capture period of 33 min (1980 s) was chosen. This takes into account potentially erroneous data at the very beginning of the capture due to the stochasticity of the freezing event. A capture length of 33 min ensures at least 30 min of good data for every experiment, while still being long to enough to allow for observable recrystallisation. The large video files were then further processed as only one in sixty frames were kept. This meant that one second in the final video file corresponded to one minute real time. This was primarily done to conserve hard drive space and reduce processing time. See 8.2.

The final data is trimmed and aligned, so that the initial crystallisation event happens at t = 0 and the last frame is at t = 30 min.

[3] FFMPEG, open source multimedia framework. https://www.ffmpeg.org/.

2.4.2. Processing with an open source image analysis platform: FIJI

The compressed video file was imported to FIJI [23] with each second consisting of 25 frames, resulting in a total of 825 analysed frames per experiment (Fig. 3a).

Each frame was then automatically processed using the FIJI functions described in Fig. 3. See 8.3 for code details. Each frame had it's colors saturated to enhance contrast (Fig. 3b). Areas of high contrast were located and deemed edges, to separate bulk crystal and interface (Fig. 3c). A threshold value for edges was set, so that the image could be converted into a binary mask of the original (Fig. 3d).

At this stage, recrystallisation results in large open areas, corresponding to bulk crystal surface.

Various artifacts from the video recording were removed using the despeckle function, which removes single pixels from areas of opposite value. The noise removal function removes one pixel from the boundary between black and white (Fig. 3e). The dilate function was used to compensate for the removal of pixels by the despeckle function (Fig. 3f). As the images then only consisted of black and white pixels, it was possible to count each type and place them on a map. A black pixel typically represents bulk crystal, and white pixels are either noise or edges between crystals. The "Distance map" function was used to count the largest distances between bulk and edge, as represented by white and black pixels, respectively (Fig. 3g). The distance map result therefore represents the largest crystal radius, assuming all crystals are circular. A ratio of 1.98 pixels/μm was used to convert data to crystal sizes, that were then plotted against time (Fig. 3h).

3. Results

For results pertaining to the function of the cryostage, cooling potential and efficiency, see the accompanying Data in Brief article [2].

Here we present the first recrystallisation data made with the OSC, comparing it to data collected using a Clifton nanolitre osmometer as cryostage.

3.1. Recrystallisation detection

Fig. 4 shows two sets of recrystallisation experiments. One set was produced on the Clifton nanoliter osmometer and the other was produced with the OSC. The OSC results are denoted with "*" in Fig. 4. The initial crystal radius of the rmAFP256 experiments differed, but did not change significantly throughout the experiment duration. One control (rmAFP2048*) grew larger crystals than the remaining sets of controls, but was still easily distinguishable from the samples containing AFP at active concentrations. So while there were inherent variations within the control samples, the final result did not change.

Fig. 5 summarises the results in Fig. 4 by only showing the difference between the average max crystal radius during the first minute and the 30th minute, hence the name ΔR_{30} (see Fig. 5).

ANOVA with post-hoc TukeyHSD on the ΔR_{30} data showed that the two rmAFP256 experiments were significantly different from all other samples, but were themselves indistinguishable from one another. Results are also summarised as significance groups in Fig. 5.

4. Discussion

Because ice recrystallisation has a profound impact on frozen foods, finding new and cheaply available sources of ice recrystallisation inhibiting proteins should be of interest to the food industry. The goal of this project was to develop: a; an open source cryostage

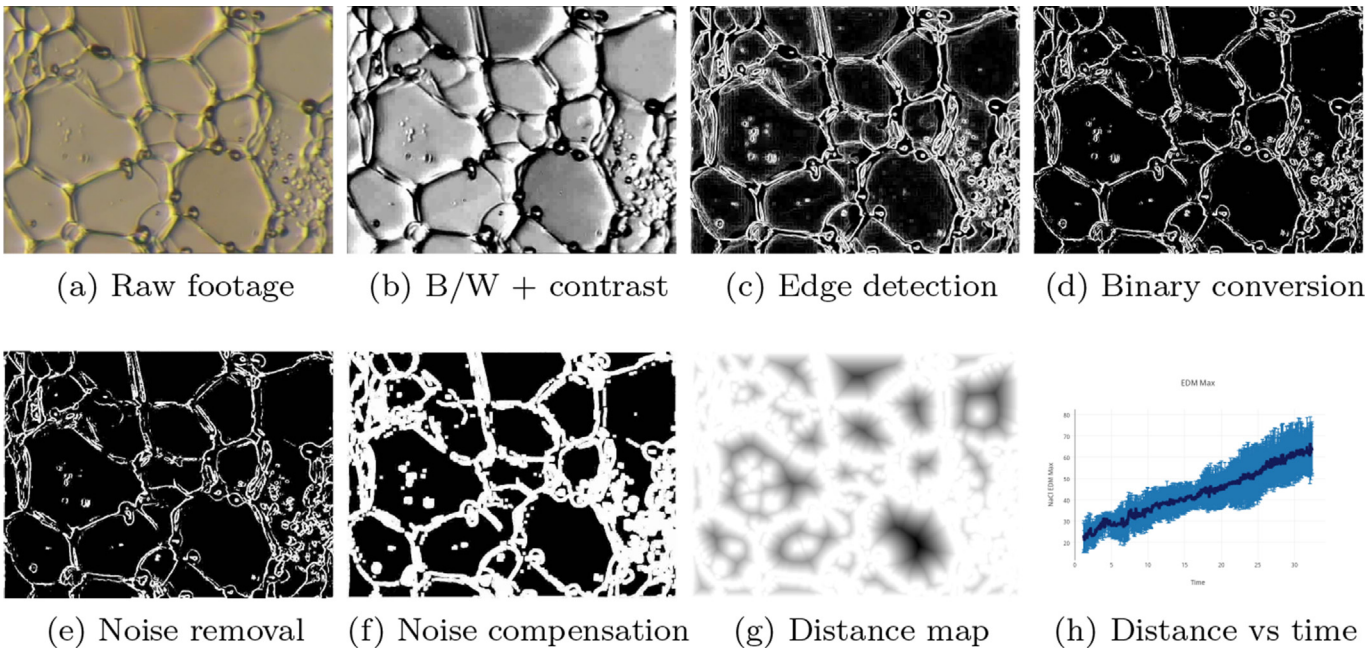

Fig. 3. Visual overview of the image processing macro. The raw input video file is converted to quantifiable data through a series of operations. From panel (a) through (h); a: Raw input, b: Greyscale conversion with increased contrast, c: Edge regions highlighted, d: Threshold conversion to binary mask, e: Despeckled image with less noise, f: Dilated image to counter despeckle, g: Euclidian distance map analysis, h: Plot of maximum crystal radius over time.

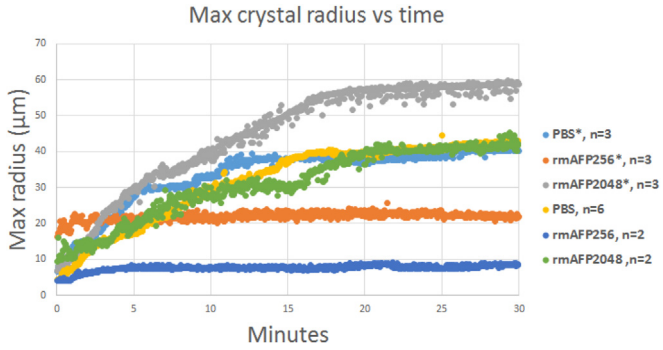

Fig. 4. Evolution of maximum crystal radius for 30 min after initial freezing event. * denotes experiments performed on the OSC, data with no notation were obtained on the Clifton nanolitre osmometer. Temperature profiles were identical. n denotes number of replicates.

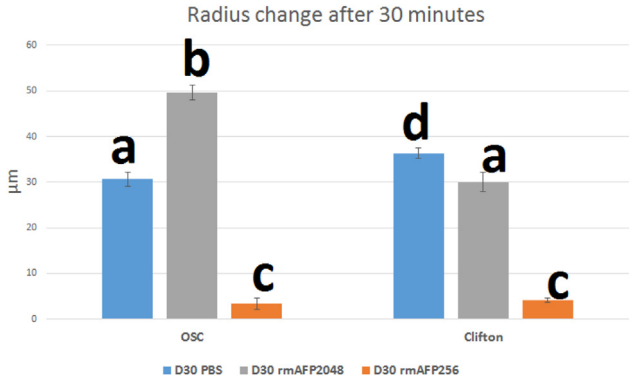

Fig. 5. Change in max crystal radius from t = 0 to t = 30, ΔR30. Letters denote statistically significant groupings.

capable of performing ice recrystallisation inhibition experiments and b; a workflow for analysis of said experiments. By simplifying the procedure required for detection of AFP, this project seeks to empower AFP researchers with a simplified and less costly setup. A genuine Arduino Uno rev 3, which was used for in this project, can be acquired for around $ 30, and the cost of assembly for the entire temperature controller setup is less than $ 150, see Section 10 and Table 1. New AFPs will hopefully be discovered more frequently, with increased accessibility of experimental hardware and software. Results obtained on the OSC were compared to a commercial temperature controller, in the form of the Clifton nanolitre osmometer.

4.1. Recrystallisation detection

From the recording of every experiment and the results presented in Fig. 4 it is clear which samples contain a recrystallisation inhibiting agent. The results were summarised as the difference between the first and last minute in Fig. 5, and were shown to be statistically significant. For the purpose of detecting antifreeze proteins, an experimental length of 30 min is likely excessive. The lower limit of experimental length where Δr of the controls and AFP samples are significantly different was tested using the same ANOVA and TukeyHSD functions as those seen in Fig. 5. It showed that AFP and controls were significantly different after only two minutes in both experimental setups. For the purpose of detecting antifreeze activity, two minutes should theoretically be enough. For samples with very little AFP activity, longer experiments are advisable to avoid ambiguity.

The OSC can be considered a prototype at the time of writing. While an experimental temperature can be precisely calculated for each sample at a desired ice fraction, the temperature feedback and control is not completely able to follow suit. The OSC uses a very

Table 1
Estimated cost of materials used in the open source cryostage.

Item	Cost (USD)
Peltier module	36
5× PCB	20
Metal	9
Screws and bolts	5
Electronic components	5
Styrofoam	2
Pipe fitting	3
Arduino Uno	29
LCD	22
Power adapters	15
Total	146

simple voltage divider circuit to accomplish temperature readings, and these readings are dependant upon the resolution of the ADC[4] on the Arduino, which is 1024 levels. With a temperature range of 100 °C, this makes for a theoretical accuracy of 0.1 °C. Combined with background noise and uncertainty, the accuracy is probably closer to 0.2 °C. This problem can easily be solved by using different components, such as a higher resolution ADC or higher quality thermistors. The controller circuit for the Peltier unit could also be greatly improved by fine tuning the PID algorithm and optimising the electrical connections on the PCB, to ensure lower resistance. However, in the case of recrystallisation detection, these uncertainties are of low concern. The OSC must be able to freeze the sample at a high cooling rate and keep a set temperature, with no fluctuations. At the time of writing, it does these two things very well. When compared to the Clifton nanolitre osmometer, results acquired on either setup is fit for recrystallisation detection.

Future iterations of the OSC may include temperature control, that is precise enough to perform measurements of thermal hysteresis.

4.2. Analysis method

The results presented in this work are evolution of maximum crystal radius over time. In some cases, average crystal size may be preferable, especially if a large FOV is available. The datasets collected here were also analysed using average crystal size, and while the overall results did not change, less experimental time is required when comparing maximum crystal size, in order to get significant differences. With access to high quality and high resolution video, average crystal size should be the parameter used for comparison, such as the data analysis seen in Jackman et al. [13] and Budke et al. [3]. If crystal growth rate is of interest, using maximum crystal size creates less noise in the final results. At present, only one 60th of the original data is represented in each data set. This trimming is done to lighten the computational load presented by each data set. The data could likely be trimmed further, as 750 images per experiment is still overwhelming without the proper tools for data handling.

5. Conclusion

The open source cryostage was tested on a set of samples containing both PBS and antifreeze proteins. It was shown to be capable of producing data that resembles that of a commercial solution. For simple IRI studies, the open source cryostage can effectively replace commercial solutions, even in this early version.

The analysis scheme was subject to data from both the open source and a commercial solution. And while not completely identical, the data sets were similar enough to show that the automated analysis was capable of producing good results. There were clear differences between samples with antifreeze activity, and samples containing no antifreeze agents. It is possible to view the entire experiment as it unfolds, or simply summarise to ΔR_{30}. The results shown here are all based on largest crystal within the FOV, but the analysis method can very easily be changed to instead produce average crystal radius.

Development is ongoing and can be followed at https://github.com/pechano/cryostage, where schematics, code, PCB layout and analysis macros can be downloaded.

Conflict of interest

None.

Acknowledgments

This work was supported by the Danish Research Council for Technology and Production Sciences, grant #10-082261.

Appendix A. Supplementary data

Supplementary data related to this article can be found at http://dx.doi.org/10.1016/j.cryobiol.2016.03.010.

References

[1] I. Braslavsky, R. Drori, LabVIEW-operated novel nanoliter osmometer for ice binding protein investigations, J. Vis. Exp. JoVE (Feb. 2013) e4189(72). URL, http://www.ncbi.nlm.nih.gov/pmc/articles/PMC3597038/.
[2] J.L. Buch, H. Ramløv, Testing the Thermal and Electrical Limits of the Open Source Cryostage (Data in Brief, submitted), Feb. 2016.
[3] C. Budke, A. Dreyer, J. Jaeger, K. Gimpel, T. Berkemeier, A.S. Bonin, L. Nagel, C. Plattner, A.L. DeVries, N. Sewald, T. Koop, Quantitative efficacy classification of ice recrystallization inhibition agents, Cryst. Growth Des. 14 (9) (Sep. 2014) 4285–4294. URL, http://pubs.acs.org/doi/abs/10.1021/cg5003308.
[4] C. Budke, C. Heggemann, M. Koch, N. Sewald, T. Koop, Ice recrystallization kinetics in the presence of synthetic antifreeze glycoprotein analogues using the framework of LSW theory, J. Phys. Chem. B 113 (9) (Mar. 2009) 2865–2873. URL, http://dx.doi.org/10.1021/jp805726e.
[5] J.F. Carpenter, T.N. Hansen, Antifreeze protein modulates cell survival during cryopreservation: mediation through influence on ice crystal growth, Proc. Natl. Acad. Sci. 89 (19) (Oct. 1992) 8953–8957. URL, http://www.pnas.org/content/89/19/8953.
[6] D.S. Friis, J.L. Johnsen, E. Kristiansen, P. Westh, H. Ramløv, Low thermodynamic but high kinetic stability of an antifreeze protein from Rhagium mordax, Protein Sci. A Publ. Protein Soc. 23 (6) (Jun. 2014) 760–768. URL, http://www.ncbi.nlm.nih.gov/pmc/articles/PMC4093952/.
[7] M. Griffith, C. Lumb, S.B. Wiseman, M. Wisniewski, R.W. Johnson, A.G. Marangoni, Antifreeze proteins modify the freezing process, Planta. Plant Physiol. 138 (1) (May 2005) 330–340. URL, http://www.plantphysiol.org/content/138/1/330.
[8] R. Gupta, R. Deswal, Low temperature stress modulated secretome analysis and purification of antifreeze protein from Hippophae rhamnoides, a Himalayan wonder plant, J. Proteome Res. 11 (5) (May 2012) 2684–2696. URL, http://dx.doi.org/10.1021/pr200944z.
[9] R. Gupta, R. Deswal, Antifreeze proteins enable plants to survive in freezing conditions, J. Biosci. 39 (5) (Dec. 2014) 931–944. URL, http://link.springer.com/article/10.1007/s12038-014-9468-2.
[10] Y. Hagiwara, H. Aomatsu, Supercooling enhancement by adding antifreeze protein and ions to water in a narrow space, Int. J. Heat Mass Transf. 86 (Jul. 2015) 55–64. URL, http://linkinghub.elsevier.com/retrieve/pii/S0017931015002215.
[11] D.O. Halwani, K.G.M. Brockbank, J.G. Duman, L.H. Campbell, Recombinant Dendroides canadensis antifreeze proteins as potential ingredients in cryopreservation solutions, Cryobiology 68 (3) (Jun. 2014) 411–418. URL, http://www.sciencedirect.com/science/article/pii/S0011224014000686.
[12] R. Hightower, C. Baden, E. Penzes, P. Lund, P. Dunsmuir, Expression of antifreeze proteins in transgenic plants, Plant Mol. Biol. 17 (5) (Nov. 1991) 1013–1021 wOS: A1991GM46200006.
[13] J. Jackman, M. Noestheden, D. Moffat, J.P. Pezacki, S. Findlay, R.N. Ben, Assessing antifreeze activity of AFGP 8 using domain recognition software, Biochem. Biophys. Res. Commun. 354 (2) (Mar. 2007) 340–344. URL, http://linkinghub.elsevier.com/retrieve/pii/S0006291X06028014.

[4] Analog-to-digital converter.

[14] C. Knight, D. Wen, R. Laursen, Nonequilibrium antifreeze peptides and the recrystallization of ice, Cryobiology 32 (1) (Feb. 1995) 23–34 wOS: A1995QF43900002.
[15] E. Kristiansen, C. Wilkens, B. Vincents, D. Friis, A.B. Lorentzen, H. Jenssen, A. Løbner-Olesen, H. Ramløv, Hyperactive antifreeze proteins from longhorn beetles: some structural insights, J. Insect Physiol. 58 (11) (November 2012) 1502–1510. URL, http://linkinghub.elsevier.com/retrieve/pii/S0022191012002314.
[16] E. Kristiansen, K.E. Zachariassen, The mechanism by which fish antifreeze proteins cause thermal hysteresis, Cryobiology 51 (3) (Dec. 2005) 262–280. URL, http://www.sciencedirect.com/science/article/pii/S0011224005001215.
[17] A.J. Middleton, C.B. Marshall, F. Faucher, M. Bar-Dolev, I. Braslavsky, R.L. Campbell, V.K. Walker, P.L. Davies, Antifreeze protein from freeze-tolerant grass has a Beta-roll fold with an irregularly structured ice-binding site, J. Mol. Biol. 416 (5) (Mar. 2012) 713–724. URL, http://www.sciencedirect.com/science/article/pii/S0022283612000861.
[18] O. Mizrahy, M. Bar-Dolev, S. Guy, I. Braslavsky, Inhibition of ice growth and recrystallization by zirconium acetate and zirconium acetate hydroxide, PLoS ONE 8 (3) (Mar. 2013) e59540. URL, http://www.ncbi.nlm.nih.gov/pmc/articles/PMC3605400/.
[19] N. Pertaya, C.B. Marshall, Y. Celik, P.L. Davies, I. Braslavsky, Direct visualization of spruce budworm antifreeze protein interacting with ice crystals: Basal plane affinity confers hyperactivity, Biophys. J. 95 (1) (Jul. 2008) 333–341 wOS:000256668200033.
[20] H. Ramlov, Microclimate and variations in haemolymph composition in the freezing-tolerant New Zealand alpine weta Hemideina maori Hutton (Orthoptera:Stenopelmatidae), J. Comp. Physiol. B Biochem. Syst. Environ. Physiol. 169 (3) (Apr. 1999) 224–235 wOS:000080092400010.
[21] H. Ramløv, D.A. Wharton, P.W. Wilson, Recrystallization in a freezing tolerant antarctic nematode,Panagrolaimus davidi,and an alpine Weta,Hemideina maori(Orthoptera; stenopelmatidae), Cryobiology 33 (6) (Dec. 1996) 607–613. URL, http://www.sciencedirect.com/science/article/pii/S0011224096900644.
[22] J.A. Raymond, A.L. DeVries, Adsorption inhibition as a mechanism of freezing resistance in polar fishes, Proc. Natl. Acad. Sci. U. S. A. 74 (6) (Jun. 1977) 2589–2593.
[23] J. Schindelin, I. Arganda-Carreras, E. Frise, V. Kaynig, M. Longair, T. Pietzsch, S. Preibisch, C. Rueden, S. Saalfeld, B. Schmid, J.-Y. Tinevez, D.J. White, V. Hartenstein, K. Eliceiri, P. Tomancak, A. Cardona, Fiji: an open-source platform for biological-image analysis, Nat. Methods 9 (7) (Jul. 2012) 676–682. URL, http://www.nature.com/nmeth/journal/v9/n7/full/nmeth.2019.html.
[24] S.D. Schoville, R.A. Slatyer, J.C. Bergdahl, G.A. Valdez, Conserved and narrow temperature limits in alpine insects: thermal tolerance and supercooling points of the ice-crawlers, Grylloblatta (Insecta: grylloblattodea: Grylloblattidae), J. Insect Physiol. 78 (Jul. 2015) 55–61. URL, http://www.sciencedirect.com/science/article/pii/S0022191015000980.
[25] A.J. Scotter, C.B. Marshall, L.A. Graham, J.A. Gilbert, C.P. Garnham, P.L. Davies, The basis for hyperactivity of antifreeze proteins, Cryobiology 53 (2) (Oct. 2006) 229–239 wOS:000241145300008.
[26] M. Webb, M. Uemura, P. Steponkus, A comparison of freezing-injury in Oat and Rye – 2 cereals at the extremes of freezing tolerance, Plant Physiol. 104 (2) (Feb. 1994) 467–478 wOS: A1994MW91800022.
[27] C. Wilkens, H. Ramløv, Seasonal variations in antifreeze protein activity and haemolymph osmolality in larvae of the beetle Ragium mordax (Coleoptera: cerambycidae), Cryo Lett. 29 (4) (Aug. 2008) 293–300.
[28] D.W. Wu, J.G. Duman, Activation of antifreeze proteins from larvae of the beetle Dendroides canadensis, J. Comp. Physiol. B 161 (3) (Jul. 1991) 279–283. URL, http://link.springer.com.molly.ruc.dk/article/10.1007/BF00262309.
[29] K.E. Zachariassen, The role of polyols and nucleating agents in cold-hardy beetles, J. Comp. Physiol. 140 (3) (Sep. 1980) 227–234. URL, http://link.springer.com/article/10.1007/BF00690407.
[30] K.E. Zachariassen, J.G. Baust, R.E. Lee Jr., A method for quantitative determination of ice nucleating agents in insect hemolymph, Cryobiology 19 (2) (Apr. 1982) 180–184. URL, http://www.sciencedirect.com/science/article/pii/0011224082901390.
[31] K.E. Zachariassen, J.A. Husby, Antifreeze effect of thermal hysteresis agents protects highly supercooled insects, Nature 298 (5877) (Aug. 1982) 865–867. URL, http://www.nature.com/doifinder/10.1038/298865a0.
[32] K.E. Zachariassen, N.G. Li, A.E. Laugsand, E. Kristiansen, S.A. Pedersen, Is the strategy for cold hardiness in insects determined by their water balance? A study on two closely related families of beetles: cerambycidae and Chrysomelidae, J. Comp. Physiol. B 178 (8) (Jun. 2008) 977–984. URL, http://link.springer.com.molly.ruc.dk/article/10.1007/s00360-008-0284-6.
[33] C. Zhang, H. Zhang, L. Wang, H. Gao, X.N. Guo, H.Y. Yao, Improvement of texture properties and flavor of frozen dough by carrot (Daucus carota) antifreeze protein supplementation, J. Agric. Food Chem. 55 (23) (Nov. 2007) 9620–9626. URL, http://dx.doi.org/10.1021/jf0717034.
[34] X.-L. Zheng, L.-J. Zhou, W. Lu, Z.-H. Xian, Z.-D. Yang, C.-L. Lei, X.-P. Wang, Cold-Hardiness mechanisms in third instar larvae of spodoptera exigua Hübner (Lepidoptera: Noctuidae), Afr. Entomol. 22 (4) (Dec. 2014) 863–871. URL, http://www.bioone.org.molly.ruc.dk/doi/abs/10.4001/003.022.0401.